REGGE POLES IN QCD

A. B. KAIDALOV
Institute of Theoretical and Experimental Physics, B.Cheremushkinskaya 25, Moscow 117259, RUSSIA
E-mail: kaidalov@vitep5.itep.ru

Basic properties of Regge poles are reviewed. Regge poles are considered from both t-channel and s-channel points of view. The main part of the review is devoted to the Regge poles in QCD. The method of the Wilson-loop path integral is used to calculate trajectories of Regge poles for $q-\bar{q}$ and gluonic states. The problem of the Pomeron in QCD is discussed in details. It is shown how to use the $1/N$-expansion for classification of reggeon diagrams in QCD. The role of Regge cuts in reggeon theory is discussed and their importance for high-energy phenomenology is emphasized. Models based on the reggeon calculus, 1/N-expansion in QCD and string picture of interactions at large distances are reviewed and are applied to a broad class of phenomena in strong interactions. It is shown how to apply the reggeon approach to small-x physics in deep inelastic scattering.

1 Introduction

Regge poles have been introduced in particle physics in the beginning of 60-ies [1,2] and up to present time are widely used for description of high-energy interactions of hadrons and nuclei. Regge approach establishes an important connection between high energy scattering and spectrum of particles and resonances. It served as a basis for introduction of dual and string models of hadrons. A derivation of Regge poles in QCD is a difficult problem closely related to the nonperturbative effects in QCD and the problem of confinement. In this review I shall first remind the main properties of Regge poles. In the section 3 I shall address the problem of Regge poles in QCD using the 1/N - expansion. It will be shown now to relate QCD diagrams to reggeon theory based on analyticity and unitarity. First attempts to calculate Regge trajectories in QCD, using the nonperturbative method of Wilson-loop path integral will be reviewed. A special attention will be devoted to the problem of the Pomeron - a Regge pole which determines an asymptotic behavior of high-energy diffractive processes. This problem is closely connected to a calculation of spectra of glueballs in QCD. An analytic formula for masses of glueballs will be obtained and compared to the results of recent lattice calculations. It will be shown that mixing of gluonic and light $q\bar{q}$-states is important for the Pomeron trajectory in the small t region. A role of small distance dynamics and results of recent perturbative calculations of the Pomeron will be discussed briefly. In the Section 5 the properties of Regge cuts will be discussed and it will be

shown that these singularities play an important role at high energies. The last section will be devoted to the physics of low-x deep inelastic scattering. This interesting kinematical region has been recently studied experimentally at HERA accelerator. It will be shown how the reggeon theory and QCD evolution effects allow to understand the properties of the structure function of the proton and diffractive dissociation of a virtual photon in a broad region of virtualities Q^2.

2 Regge poles and their properties

2.1 The reggeon concept

The complex angular momentum method was first introduced by Regge in nonrelativistic quantum mechanics.[3] In relativistic theory it connects a high energy behavior of scattering amplitudes with the singularities in the complex angular momentum plane of the partial wave amplitudes in the crossed (t) channel. This method is based on the general properties of the S-matrix - unitarity, analyticity and crossing. The simplest singularities are poles (Regge poles). A Regge-pole exchange is a natural generalization of a usual exchange of a particle with spin J to complex values of J. So this method established an important connection between high energy scattering and the spectrum of hadrons. This is a t-channel point of view on Regge poles. On the other hand asymptotic behavior of scattering amplitudes at very high energies is closely related to the multiparticle production. This is the s-channel point of view on reggeons.

Let us consider first the t-channel point of view in more details.

The binary reaction $1+2 \to 3+4$ (Fig.1) is described by the amplitude $T(s,t)$, which depends on invariants $s = (p_1+p_2)^2$ and $t = (p_1-p_3)^2$. At high energies $s \gg m^2$ and fixed momentum transfer $t \sim m^2$ an exchange by a particle of spin J in the t-channel (Fig.2a)) leads to an amplitude of the form

$$T(s,t) = g_{13} \cdot g_{24} \cdot (s)^J / (M_J^2 - t) \tag{1}$$

where g_{ik} are the coupling constants and M_J is the mass of the exchanged particle.

For a partial wave expansion of amplitudes

$$f(s, cos\theta) = \frac{T(s,t)}{8\pi\sqrt{s}} = \frac{1}{p}\sum_{l=0}^{\infty}(2l+1) f_l(s) P_l(cos\theta) \tag{2}$$

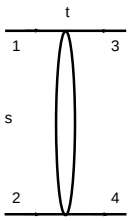

Figure 1: A diagram for a binary reaction.

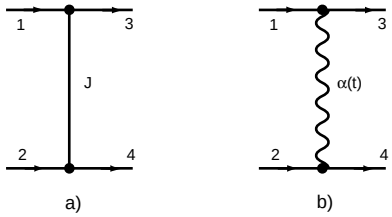

Figure 2: a) Exchange by a particle of spin J in the t-channel. b) Exchange by a Regge pole in the t-channel.

the unitarity relation leads to the constraints

$$\Im f_l(s) \geq \mid f_l(s) \mid^2; \qquad \mid f_l(s) \mid \leq 1 \tag{3}$$

It follows from eq.(1) that for an exchange of a particle with a spin $J \geq 2$ the partial wave amplitude increases with energy $\sim s^{(J-1)}$ for large s and violates unitarity as $s \to \infty$. This problem can be solved by introduction of Regge poles. It should be taken into account that the expression (1) for the amplitude is valid, strictly speaking, only close to the pole position $t \approx M_J^2$ and can be strongly modified away from the pole. Regge pole model gives an exact form of this modification and absorbs in itself exchanges by states of different spins (Fig2b)). The corresponding amplitude has the form

$$T(s,t) = f_{13}(t) \cdot f_{24}(t) \cdot (s)^{\alpha(t)} \cdot \eta(\alpha(t)) \tag{4}$$

where $\alpha(t)$ is the Regge-trajectory, which is equal to spin J of the corresponding particle at $t = M^2$. The function $\eta(\alpha(t)) = -(1+\sigma exp(-i\pi\alpha(t))/\sin(\pi\alpha(t))$ is a signature factor and $\sigma = \pm 1$ is a signature. It appears due to the fact that in relativistic theory it is necessary to consider separately analytic continuation of partial wave amplitudes in the t-channel to complex values of angular momenta

J from even ($\sigma = +$) and odd ($\sigma = -$) values of J. This factor is closely related to the crossing properties of scattering amplitudes under interchange of s to $u = (p_1 - p_4)^2$. Amplitudes with $\sigma = +$ are even under the interchange $s \leftrightarrow u$ ($s \leftrightarrow -s$ for high energies), while for $\sigma = -$ amplitudes are antisymmetric under this operation. It should be emphasized that the single Regge exchange corresponds to an exchange of particles or resonances which are "situated" on the trajectory $\alpha(t)$. For example if $\alpha(t) = J$, where J is an even (odd) integer for $\sigma = +(-)$ for $t = M_J^2$ and M_J^2 is less than the threshold for transition to several hadrons ($4m_\pi^2$ for particles which can decay into two pions), then the Regge amplitude eq.(4) transforms into the particle exchange amplitude eq.(1) with $g_{13}g_{24} = f_{13}(M_J^2) \cdot f_{24}(M_J^2) 2/\pi\alpha'(M_J^2)$.

If M_J is larger than the threshold value then $\alpha(t)$ is a complex function and can be written for $t \approx M_J^2$ in the form

$$\alpha(t) = J + \alpha'(M_J^2) \cdot (t - M_J^2) + iIm\alpha(M_J^2) \tag{5}$$

In this case for $Im\alpha(M_J^2) \ll 1$ Regge pole amplitude eq.(4) corresponds to an exchange in the t-channel by a resonance and has the Breit-Wigner form

$$T(s,t) = -g_{13} \cdot g_{24}(s)^J/(t - M_J^2 + iM_J\Gamma_J) \tag{6}$$

with a width $\Gamma_J = Im\alpha(M_J^2)/M_J\alpha'(M_J^2)$.

Thus a reggeization of particle exchanges leads to a natural resolution of the above mentioned problem with a violation of the unitarity, -Regge trajectories, which correspond to particles with high spins can have $\alpha(t) \leq 1$ in the physical region of high energy scattering $t < 0$ and the corresponding amplitudes will increase with s not faster than s^1, satisfying the unitarity. The experimental information on spectra of hadrons and high energy scattering processes nicely confirms this theoretical expectation. The only exception is the Pomeranchuk pole (or the Pomeron), which determines high energy behavior of diffractive processes. I shall pay a special attention to properties of the Pomeron in this review.

2.2 Bosonic and fermionic Regge poles, vacuum exchange

Let us consider the main properties of Regge poles.
a)Factorization. Regge poles couple to external particles in a factorizable way, which is manifest in eq.(4).
b)Regge poles have definite conserved quantum numbers like the baryon quantum number, parity P, isospin e.t.c. As it was mentioned above they have also a definite signature σ.

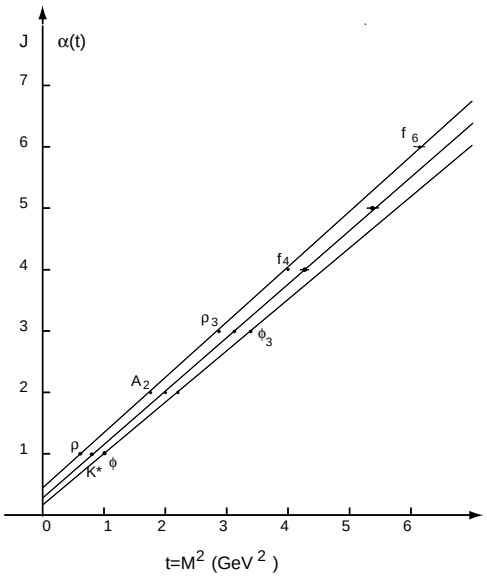

Figure 3: Trajectories for some well-known Regge poles.

An information on trajectories of Regge poles can be obtained for $t < 0$ from data on two-body reactions at large s and for $t > 0$ from our knowledge of the hadronic spectrum. We have seen that a bosonic trajectory corresponds to particles and resonances for those values of t where it passes integer values ($Re\alpha(t) = n$) even for $\sigma = +$ and odd for $\sigma = -$. While for fermionic trajectories particles correspond to $Re\alpha(t) = \frac{n}{2} = J$ and signature $\sigma = (-1)^{J-\frac{1}{2}}$. There can be many trajectories with the same quantum numbers indicated above, which differ by a quantum number analogous to the radial quantum number. Such trajectories are usually called "daughter" trajectories and masses of corresponding resonances (with the same value of J) for them are higher than those for the leading trajectory with given quantum numbers.

Trajectories for some well established bosonic Regge poles are shown in Fig.3. Note that all these trajectories have $\alpha_i(0) \leq 0.5$ for $t \leq 0$. One of the most interesting properties of these trajectories is their surprising linearity. This usually interpreted as a manifestation of strong forces between quarks at large distances, which lead to color confinement. The linearity of Regge trajectories indicates to a string picture of the large distance dynamics between quarks and it was a basis of dual models for hadronic interactions. Other

properties of mesonic Regge trajectories, which are evident from Fig.3 are exchange and isospin degeneracies, - trajectories with different signatures and I=0 or I=1 (but with the same σP) are degenerate with a good accuracy (at least in the region $t > 0$). This is also in an agreement with dual models or approaches based on 1/N-expansion in QCD. In dual or string models of hadrons the daughter trajectories must be parallel to the leading one and displaced in the j-plane by integers. Experimental information on the daughter trajectories is rather limited but it does not contradict to these predictions.

Information on mesonic Regge trajectories in the region of negative t, obtained from an analysis of binary reactions at high energies fits quite well the lines shown in Fig.3 obtained from the spectrum of resonances. The most detailed information exists for ρ and A_2-trajectories, which contribute to the reactions $\pi^- p \to \pi^0 n$ and $\pi^- p \to \eta n$ correspondingly.

Fermionic Regge trajectories are in general analytic functions of $W = \sqrt{t}$ and using the analyticity properties of the corresponding partial-wave amplitudes it is possible to show that there must be pairs of trajectories with different parity, which satisfy to the condition

$$\alpha_+(W) = \alpha_-(-W) \tag{7}$$

Experimental data on spectrum of baryons show that baryonic trajectories as well as mesonic ones are nearly straight lines in variable t with the universal slope $\alpha' \approx 1 GeV^{-2}$. This universality of the slopes is natural in the string picture of baryons with a quark and a diquark at the ends. However, according to eq.7 the fermionic trajectory, which is linear in $t = W^2$, does not change as $W \to -W$ and thus should coincide with its parity partner. This in its turn leads to parity doubling of states on this Regge trajectory. Experimentally there are many baryonic states with the same spin and different parity, which are nearly degenerate in mass. However there are no partners for the lowest states (N, Δ) on these trajectories. This pattern of baryonic Regge trajectories is not yet understood theoretically. The relation 7 is a consequence of analyticity in relativistic quantum theory, but it is not realized in the existing quark models of baryons.

At the end of this section I shall discuss properties of the pole which has a special status in the Regge approach to particle physics - the Pomeranchuk pole or the Pomeron. This pole was introduces into theory in order account for diffractive processes at high energies. In the Regge pole model an amplitude of high energy elastic scattering has the form of eq.(4) and the total interaction cross section, which by the optical theorem is connected to $ImT(s, 0)$, can be

written as a sum of the Regge poles contributions

$$\sigma^{tot}(s) = \sum_k b_k(0)(s)^{\alpha_k(0)-1} \tag{8}$$

The poles, which are shown in Fig.3 have $\alpha_k(0) < 1$ and thus their contributions to $\sigma^{tot}(s)$ decrease as a $s \to \infty$. However experimental data show that at $s \sim 100\ GeV^2$ total cross sections of hadronic interactions have a weak energy dependence and they slowly (logarithmically) increase with energy at higher energies. In the Regge pole model this can be related to the pole, which has an intercept $\alpha_P(0) \approx 1$. This pole is usually called Pomeron or the vacuum pole, because it has the quantum numbers of the vacuum, - positive signature, parity and G (or C) parity and isospin I=0.

It is believed that in QCD this pole is related to gluonic exchanges in the t-channel. So it is usually assumed that gluonium states correspond to this trajectory in the region of positive t. We shall discuss possible relation between QCD and Regge theory in more details in the next chapters.

A value of intercept of the Pomeranchuk pole is of crucial importance for the Regge theory. If $\alpha_P(0) = 1$, as it was assumed initially, then all the total interaction cross sections tend to a constant at very high energies. This theory has however some intrinsic difficulties and must satisfy to many constraints in order to be consistent with unitarity. Besides experimental data indicate that $\sigma_{hN}^{(tot)}$ rise with energy. This logarithmic increase of total cross sections at very high energies is in accord with $ln^2 s$ behavior consistent with the Froissart theorem.[4] Thus at present the supercritical Pomeron theory with $\alpha_P(0) > 1$ is widely used. In a model with only Regge poles taken into account an assumption that $\alpha_P(0) > 1$ would lead to a power like increase of total cross sections, thus violating the Froissart bound. However in this case other singularities in the j- plane,- moving branch points should be taken into account and their contributions allow one to restore unitarity and to obtain the high energy behavior of scattering amplitudes which satisfy to the Froissart bound. Properties of these moving cuts are considered in the section 5.

Let us note that the Pomeranchuk singularity has a positive signature, so it gives equal contribution to amplitudes for elastic scattering of particle and antiparticle. Thus it automatically satisfies to the Pomeranchuk theorem on asymptotic equality of total interaction cross sections for particle and antiparticle. A difference between these amplitudes in the Regge model is connected to poles with negative signature (like ρ and ω). It is usually assumed that the only singularities in the j-plane with negative signature are due to the known Regge poles with $\alpha_k(0) \leq 0.5$. In this case differences of cross sections for aN and $\bar{a}N$-interactions decrease with energy as $1/\sqrt{s}$. This behavior agrees

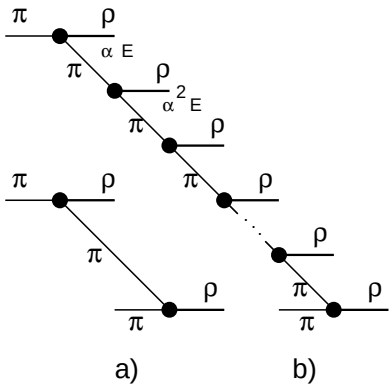

Figure 4: a) Exchange by a pion in the t-channel in the reaction $\pi\pi \to \rho\rho$. b) Diagram of multiperipheripheral production of ρ mesons .

with existing experimental information. In principle it is possible to have a singularity with negative signature at $j \approx 1$. This singularity usually called "odderon". It appears in perturbative QCD calculations.

2.3 s-channel picture of reggeons

Regge poles give contributions to imaginary parts of two-body scattering amplitudes. For the Pomeron with $\alpha_P(0) \approx 1$ the amplitude is mostly imaginary. Unitarity relates imaginary parts of two-body amplitudes to sums over intermediate states in the s-channel. So the natural question is: what are the intermediate states connected to reggeons? These are so called multiperipheral states the properties of which I shall briefly discuss now. Consider as an example the simplest inelastic process of ρ-mesons production in $\pi\pi$ collisions. The diagrams with pion exchange shown in Fig.4 give an important contribution to amplitudes of these processes. They lead to peripheral configurations - all ρ-mesons are produced with rather small momentum transfer $\sim m_\pi$. The diagram of Fig. 4a) is large only at rather low energies when the average energy of the virtual pion in the lab. system ($\sim \alpha E, \alpha \leq 1$, E-is the lab. energy of the projectile) is low enough to produce a ρ meson with a target pion. At higher energies the cross section of this process decreases with energy as $1/s^2$. At these energies it is necessary to decrease the energy of the virtual pion in several steps as it is shown in Fig.4b) in order to have a slow virtual pion at the end of the chain. If the energy decreases by a factor α at each step then after n steps it will be $\alpha^n E$ and we require that it is $\sim m_\rho$. So on average the number

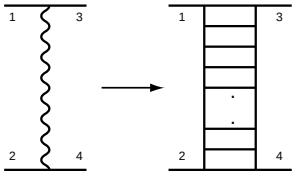

Figure 5: Reggeon as a ladder diagram.

of steps (related to the number of produced resonances) $\langle n \rangle \sim ln\frac{E}{m_\rho}/ln\frac{1}{\alpha}$.

This is an example of the diagrams of the multiperipheral model [5] of multiparticle production. Summation of these diagrams leads to the Regge-type behavior for an imaginary part of two-body amplitudes. So in this model reggeon corresponds to a sum of ladder-type diagrams shown in Fig.5. Let us consider now the multiperipheral process in the impact parameter $\vec{b}$ space. Each step has a finite size in $\vec{b} \sim 1/m_\pi$. They add independently, so there is a random walk in the $\vec{b}$-space and the average size of interaction increases with energy as

$$\bar{R}^2 \equiv \langle \vec{b}^2 \rangle \approx \frac{\bar{n}}{m_\pi^2} \sim \frac{ln\frac{E}{m_\rho}}{m_\pi^2} \tag{9}$$

The total time of development of the fluctuation in the lab. frame is large, - $\tau \sim E/m^2$.

In the multiperipheral model the hadronic final states have the following properties.

a) Short range correlations in rapidity. Particles separated by several steps of the multiperipheral process and having substantially different energies [this means that difference of rapidities $y_1 - y_2$ ($y = ln(E + p_\parallel)/m_\perp$) for these particles is large] are uncorrelated. The correlation function exponentially decreases with rapidity difference

$$c(y_1, y_2) = \frac{d\sigma}{\sigma^{in} dy_1 dy_2} - (\frac{d\sigma}{\sigma^{in} dy_1})(\frac{d\sigma}{\sigma^{in} dy_2}) \sim exp[-\lambda(y_1 - y_2)] \tag{10}$$

This property of the multiparticle final state leads to many consequences for inclusive cross sections. Consider for example single particle inclusive cross section

$$f^a \equiv E\frac{d^3\sigma^a}{d^3p} = \frac{d^2\sigma(y_1 - y_a, y_a - y_2, p_{\perp a}^2)}{dy_a d^2p_{\perp a}} \tag{11}$$

Short range correlation between particles means in this case that all inclusive densities $n^a \equiv f^a/\sigma^{in}$ are independent of $y_i - y_k$ for $y_i - y_k \gg 1$. For example

at high energies when $y_1 - y_2 \simeq ln(s/m^2) \gg 1$ in the fragmentation region of particle 1 $y_1 - y_a \sim 1$ and $y_a - y_2 \approx y_1 - y_2 \gg 1$ the density n^a becomes a function of only two variables

$$n^a = \phi(y_1 - y_a, p^2_{\perp a}) \tag{12}$$

b) The property eq.12 is equivalent to the Feynman scaling in variable $x_F = 2p_{\parallel a}/\sqrt{s} \approx exp[-(y_1 - y_a)]$

$$n^a = \phi(x_F, p^2_{\perp a}) \tag{13}$$

c) In the central rapidity region when both $y_1 - y_a$ and $y_a - y_2$ are large n^a becomes a function of only one variable $(p^2_{\perp a})$. So in this model rapidity distributions in the central region are flat .
d) The average number of produced particles $\langle n \rangle$ increases logarithmically with energy at large $ln(s/m^2)$.
e) There is a fast decrease of distributions with $p_\perp$. The form of this function depends on details of the model.
f) Multiplicity distributions of produced particles in these models have Poisson-type behavior.

$$\langle n^2 \rangle - \langle n \rangle^2 \approx c\langle n \rangle \tag{14}$$

This is a consequence of short range correlations in rapidity.

The properties of inclusive distributions listed above can be quantified in the Regge model, using Mueller-Kancheli [6] diagrams . There is a relation between a discontinuity of $3 \to 3$ forward scattering amplitude $1\bar{a}2 \to 1\bar{a}2$ and inclusive cross section f^a analogous to the optical theorem which relates a forward elastic scattering amplitude to a total cross section. For large $y_i - y_a$ $(s_{i\bar{a}} \gg m^2)$ it is possible to use the Regge pole theory, which gives predictions on energy (rapidity) dependence of inclusive cross sections. For example consider the central region of rapidities when both $y_1 - y_a \gg 1$ and $y_a - y_2 \gg 1$. In this case diagrams of double Regge limit (Fig.6) can be used and inclusive cross sections can be written as follows

$$f^a = \sum_{i,k} g^i_{11}(0) g^k_{22}(0) g^a_{ik} exp[(\alpha_i(0) - 1)(y_1 - y_a) + (\alpha_k(0) - 1)(y_a - y_2)] \tag{15}$$

These results can be easily obtained in the multiperipheral model.

2.4 Diffractive production processes

Let us consider now diffractive production of particles at high energies. In the Regge pole model these processes are described by the diagrams with Pomeron

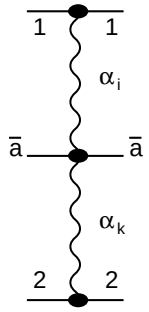

Figure 6: Regge diagram for inclusive cross section in central region.

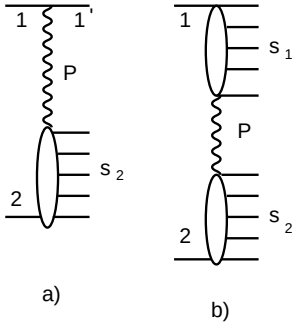

Figure 7: Diagrams for diffractive production of hadrons in the Regge pole model.

exchange (Fig.7). It is possible to have excitation of one of the colliding hadrons (Fig.7a)), - single diffraction dissociation or excitation of both initial particles,- double diffraction dissociation (Fig.7b)).

For all diffractive processes there is a large rapidity gap between groups of produced particles. For example for single diffraction dissociation there is a gap between the particle $1'$ and the rest system of hadrons. This rapidity gap $\Delta y \approx ln(1/1-x)$, where x the x_F for hadron $1'$ in Fig.7a). A mass of diffractively excited state at large s can be large. The only condition for diffraction dissociation is $s_i \ll s$. For large masses of excited states $s_2 \approx (1-x)s$ and $\xi' \approx \Delta y \approx ln(s/s_2)$.

The cross section for inclusive single diffraction dissociation in the Regge

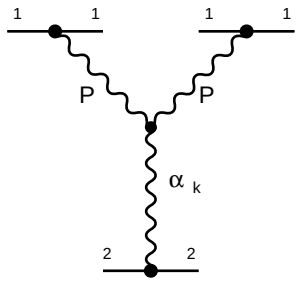

Figure 8: Triple-Regge diagram.

pole model can be written in the following form

$$\frac{d^2\sigma}{d\xi_2 dt} = \frac{(g_{11}(t))^2}{16\pi}|G_p(\xi',t)|^2\sigma_{P2}^{(tot)}(\xi_2,t) \tag{16}$$

where $\xi_2 \equiv ln(s_2/s_0)$ and $G_p(\xi',t) = \eta(\alpha_p(t))exp[(\alpha_p(t)-1)\xi']$ is the Pomeron Green function. The quantity $\sigma_{P2}^{(tot)}(\xi_2,t)$ can be considered as the Pomeron-particle total interaction cross section.[7] Note that this quantity is not directly observable one and it is defined by its relation to the diffraction production cross section (eq.16). This definition is useful however because at large s_2 this cross section has the same Regge behavior as usual cross sections

$$\sigma_{P2}^{(tot)}(s_2,t) = \sum_k g_{22}^k(0)r_{PP}^{\alpha_k}(t)(\frac{s_2}{s_0})^{\alpha_k(0)-1} \tag{17}$$

where the $r_{PP}^{\alpha_k}(t)$ is the triple-reggeon vertex (Fig.8), which describes coupling of two Pomerons to reggeon α_k.

In this kinematical region $s \gg s_2 \gg m^2$ the inclusive diffractive cross section is described by the triple-Regge diagrams of Fig.8 and has the form

$$f^1 = \sum_k G_k(t)(1-x)^{\alpha_k(0)-2\alpha_P(t)}(\frac{s}{s_0})^{\alpha_k(0)-1} \tag{18}$$

The Pomeron-proton total cross section and triple-Regge vertices r_{PP}^P, r_{PP}^f have been determined from analysis of experimental data of diffractive production of particles in hadronic collisions (see reviews [8]).

3 Mesonic Regge poles in QCD

An astonishing linearity of trajectories for Regge-poles corresponding to the known $q\bar{q}$-states indicates to an essentially nonperturbative, string-like dynamics. A nonperturbative method, which can be used in QCD for description of large distance dynamics, is the $1/N$-expansion (or topological expansion).[9,10]

In this approach the quantities $1/N_c$[9] or $1/N_{lf}$[10] (N_{lf} is the number of light flavors) are considered as small parameters and amplitudes and Green functions are expanded in terms of these quantities. In QCD $N_c = 3$ and $N_{lf} \simeq 3$ and the expansion parameter does not look small enough. However we shall see below that in most cases the expansion parameter is $1/N_c^2 \sim 0.1$.

In the formal limit $N_c \to \infty$ ($N_f/N_c \to 0$) QCD has many interesting properties and has been intensively studied theoretically. There is a hope to obtain an exact solution of the theory in this limit (2-dimensional QCD has been solved in the limit $N_c \to \infty$). However this approximation is rather far from reality, as resonances in this limit are infinitely narrow ($\Gamma \sim 1/N_c$). The case when the ratio $N_f/N_c \sim 1$ is fixed and the expansion in $1/N_f$ (or $1/N_c$) is carried out [10] seems more realistic.

This approach is called sometimes by the topological expansion, because the given term of this expansion corresponds to an infinite set of Feynman diagrams with definite topology. It should be emphasized that $1/N$-expansion should be applied to Green-functions or amplitudes for white states.

The first term of the expansion corresponds to the planar diagrams of the type shown in Fig.9 for the binary reaction. These diagrams always have as border lines the valence quarks of the colliding hadrons. At high energies they should correspond to exchanges by secondary Regge poles $\alpha_R(\rho, A_2, \omega, ...)$ "made of" light quarks. The s-channel cutting of the planar diagram of Fig.9a) is shown in Fig.9b). Here and in the following we do not show internal lines of gluons and quark loops. This diagram corresponds to a multiparticle production, which has the same properties as in the multiperipheral model. The topological classification of diagrams in QCD leads to many relations between parameters of the reggeon theory, hadronic masses, widths of resonances and total cross sections (for a review see [11]) . All these relations are in a good agreement with experiment.

A contribution of the planar diagrams to the total cross section decreases with energy as $1/s^{(1-\alpha_R(0))} \approx 1/\sqrt{s}$. This decrease is connected to the fact that quarks have spin $1/2$ and in the lowest order of perturbation theory an exchange by two quarks in the t-channel leads to the behavior $\sigma \sim 1/s$, which corresponds to the intercept $\alpha_R(0) = 0$. Interaction between quarks should lead to an increase of the intercept to the observed value $\alpha_R(0) \approx 0.5$.

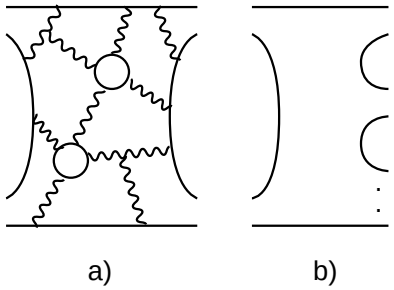

Figure 9: a) Planar diagram for binary reactions. Full lines denote quarks, wavy lines - gluons. b) Same for $12 \to X$. Internal lines of gluons and quarks are not shown.

Is it possible to calculate Regge-trajectories from QCD? Even for planar diagrams this is a difficult problem. It was considered in paper [12] using the method of Wilson-loop path integral.[13] It was shown that under a reasonable assumption about large distances dynamics: minimal area law for Wilson loop at large distances, confirmed by numerous lattice data, $\langle W \rangle \sim exp(-\sigma S_{min})$, it is possible to calculate spectrum of $q\bar{q}$-states. In these calculations virtual $q\bar{q}$-pairs and spin effects were neglected. It was shown that the mass spectrum can be determined from the following effective Hamiltonian H_0

$$H_0 = \frac{p_r^2}{\mu(t)} + \mu(t) + \frac{L(L+1)}{r^2[\mu + 2\int_0^1 (\beta - \frac{1}{2})^2 \nu d\beta]} + \\ + \int_0^1 \frac{\sigma_{adj}^2 d\beta}{2\nu(\beta,t)} r^2 + \frac{1}{2}\int_0^1 \nu(\beta,t) d\beta \qquad (19)$$

Here $\mu(t)$ and $\nu(\beta,t)$ are positive auxiliary functions which are to be found from the extremum condition.[12] Their extremal values are equal to the effective quark energy $\langle \mu \rangle$ and energy density of the adjoint string $\langle \nu \rangle$.

The resulting spectrum of H_0 for light quarks with a good accuracy is described by a very simple formula

$$\frac{M^2}{2\pi\sigma} = L + 2n_r + c_1 \qquad (20)$$

This spectrum is shown in Fig.10 and corresponds to an infinite set of linear Regge trajectories similar to the one of dual and string models.
In order to make realistic calculations of masses of hadrons which can be

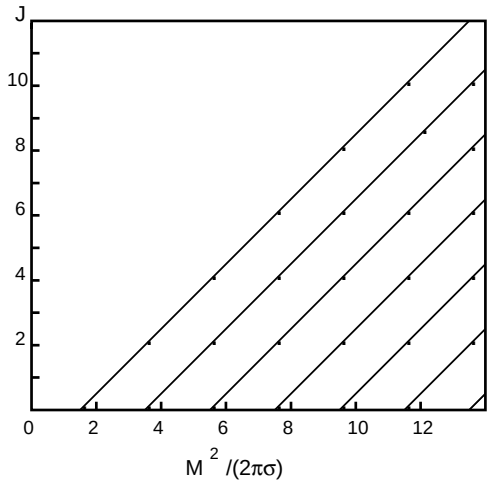

Figure 10: Calculated spectrum of $q - \bar{q}$ states and corresponding Regge-trajectories.

compared with experiment it is necessary to take into account perturbative interactions at small distances, spin effects and quark loops. For light quarks spin effects are non trivial as the spontaneous violation of the chiral symmetry should be properly taken into account.

4 Glueballs and the Pomeron in QCD

It was mentioned above that the Pomeron in QCD is usually related to gluonic exchanges in the t-channel.[14]. This is connected with the fact that gluons naturally lead to the vacuum quantum numbers and the simplest perturbation theory diagram for scattering amplitude with an exchange by 2 gluons leads to a cross section which does not depend on energy (due to spin of gluon $Sg = 1$). Thus in this approximation $\alpha_P(0) = 1$. In perturbation theory an interaction between gluons leads to an increase of the Pomeron intercept.[15]

From the point of view of 1/N-expansion the Pomeron is related to the cylinder-type diagrams, shown in Fig.11 with gluonic states (mixed with $q\bar{q}$-pairs) on a surface. In this approach the Pomeron is related to glueballs.

Glueballs are among the most intriguing objects both in experiment and theory. While experimental situation is not yet settled, lattice simulations [16,17] yield an overall consistent picture of lowest ($< 4\ GeV$) mass spectrum. The mass scale and level ordering of the resulting glueball spectra strongly differ

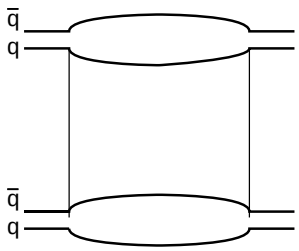

Figure 11: Cylinder-type diagrams for the Pomeron.

from those of meson spectra, yielding a unique information about the nonperturbative structure of the gluonic vacuum.

The problem of spectra of glueballs and its relation to the Pomeron was considered in papers [18,19], using the method of Wilson-loop path integral discussed above for the case of $q\bar{q}$-Regge poles.

In the approximation when the spin effects and quark loops are neglected the spectrum of two-gluon glueballs is determined by the same Hamiltonian H_0 given by eq.19 with the only difference that the string tension (σ_{fund}) for the $q\bar{q}$ system is changed to σ_{adj}. Thus the mass spectrum for glueballs is given be eq.20 with the change $\sigma \to \sigma_{adj}$.

The value of σ_{adj} in (20) can be found from the string tension σ_{fund} of $q\bar{q}$ system, multiplying it by $\frac{9}{4}$, as it follows from Casimir scaling observed on the lattices. Taking experimental Regge slope for mesons $\alpha' = 0.89\ GeV^{-2}$ one obtains $\sigma_{fund} = 0.18\ GeV^2$ and $\sigma_{adj} \approx 0.40\ GeV^2$.

In order to compare our results with the corresponding lattice calculations [16,17] it is convenient to consider the quantity $\bar{M}/\sqrt{\sigma_f}$, which is not sensitive to the choice of string tension σ. We also introduce the spin averaged mass $\bar{M}$ which for $L = 0, n_r = 0$ states is defined as $\bar{M} = \frac{1}{3}(M(0^{++}) + 2M(2^{++}))$, and in a similar way for higher states. This definition takes into account the structure of spin-splitting terms, so that $\bar{M}$ can be compared with the eigenvalues M_0 of spinless Hamiltonian eq.19.

The comparison of our predictions for spin averaged masses of the lowest glueball states with corresponding lattice results is given in Table 1. For the average mass with $L = 2, n_r = 0$ lattice results are limited to the state 3^{++}. An agreement is perfect especially for the mass of the lowest state which is calculated on lattices with highest accuracy.

Table 1
Spin averaged glueball masses $M_G/\sqrt{\sigma_f}$

Quantum numbers		This work	Lattice data	
			paper [17]	paper [16]
hline 2 gluon states	$l=0, n_r=0$	4.68	4.66±0.14	4.55±0.23
	$l=1, n_r=0$	6.0	6.36±0.6	6.1 ±0.5
	$l=0, n_r=1$	7.0	6.68±0.6	6.45±0.5
	$l=2, n_r=0$	7.0	9.0 ±0.7(3^{++})	7.7 ±0.4(3^{++})
	$l=1, n_r=1$	8.0		8.14 ±0.4(2^{*-+})
3 gluon state	K=0	7.61		8.19±0.48

Table 2
Comparison of predicted glueball masses with lattice data

J^{PC}	M(GeV)	Lattice data		$M[G]/M[0^{-+}]$		Difference
	This work	paper [16]	paper [17]	This work	paper [16]	
0^{++}	1.58	1.73±0.13	1.74±0.05	0.62	0.67(2)	-7%
0^{++*}	2.71	2.67±0.31	3.14±0.10	1.06	1.03(7)	3%
2^{++}	2.59	2.40±0.15	2.47±0.08	1.01	0.92(1)	9%
2^{++*}	3.73	3.29±0.16	3.21±0.35			
0^{-+}	2.56	2.59±0.17	2.37±0.27			
0^{-+*}	3.77	3.64±0.24		1.47	1.40(2)	5%
2^{-+}	3.03	3.1±0.18	3.37±0.31	1.18	1.20(1)	-1%
2^{-+*}	4.15	3.89±0.23		1.62	1.50(2)	8%
3^{++}	3.58	3.69±0.22	4.3±0.34	1.40	1.42(2)	-2%
1^{--}	3.49	3.85±0.24		1.36	1.49(2)	-8%
2^{--}	3.71	3.93±0.23		1.45	1.52(2)	-1%
3^{--}	4.03	4.13±0.29		1.57	1.59(4)	

The spin splittings for glueball masses were calculated in paper [19] assuming that spin effects can be treated as small perturbations. A largest correction is obtained for the lowest state from the spin-spin interaction. The results are compared with lattice calculations in the Table 2 (for $\alpha_s = 0.3$).

Let us consider now the Pomeron Regge trajectory in this approach in more details, taking into account both nonperturbative and perturbative con-

tributions to the Pomeron dynamics.

The large distance, nonperturbative contribution gives according to Eq.(20) for the leading glueball trajectory ($n_r = 0$)

$$\alpha_P(t) = -c_1 + \alpha'_P t + 2 \tag{21}$$

with $\alpha'_P = \frac{1}{2\pi\sigma_a}$.

In eq.21 spins of "constituent" gluons are taken into account, but a small nonperturbative spin-spin interactions were neglected.

For the intercept of this trajectory we obtain $\alpha_P(0) \approx 0.5$, which is substantially below the value found from analysis of high-energy interactions $\alpha_P(0) = 1.08 \div 1.2$. I would like to emphasize that contrary to interactions related to emission of real particles in the s-channel (for example emission of gluons in the perturbative ladder-type diagrams) the confining interaction considered above leads to a decrease of an intercept of a Regge trajectory compared to the Born approximation.

The most important nonperturbative source, which can lead to an increase of the Pomeron intercept is the quark-gluon mixing or account of quark-loops in the gluon "medium". In the 1/N -expansion this effect is proportional to N_f/N_c, where N_f is the number of light flavors. In the leading approximation of the $1/N_c$-expansion there are 3 Regge-trajectories with vacuum quantum numbers, - $q\bar{q}$-planar trajectories (α_f made of $u\bar{u}$ and $d\bar{d}$ quarks, $\alpha_{f'}$ made of $s\bar{s}$-quarks) and pure gluonic trajectory - α_G. The transitions between quarks and gluons $\sim \frac{1}{N_c}$ will lead to a mixing of these trajectories. Note that for a realistic case of G, f and f'-trajectories (eq.21 and Fig.3) all 3-trajectories before mixing are close to each other in the small t region. In this region mixing between trajectories is essential even for small coupling matrix $g_{ik}(t)$. Lacking calculation of these effects in QCD they were considered in the paper [19] in a semi–phenomenological manner.

Denoting by $\bar{\alpha}_i$ the bare f, f' and G–trajectories and introducing the mixing matrix $g_{ik}(t)(i,k = 1,2,3)$ we obtain the following equation for determination of resulting trajectories after mixing.[19]

$$j^3 - j^2 \sum \bar{\alpha}_i + j(\sum_{i\neq k} \bar{\alpha}_i\bar{\alpha}_k - g^2_{ik}) - \bar{\alpha}_1\bar{\alpha}_2\bar{\alpha}_3 + \sum_{i\neq k\neq l} \bar{\alpha}_l g^2_{ik} - 2g_{12}g_{13}g_{23} = 0 \tag{22}$$

For realistic values of $g_{ik}(t)$ (for details see [19]) the Pomeron intercept is shifted to the values $\alpha_P(0) \approx 1$. For $t > 1GeV^2$ the Pomeron trajectory is very close to the planar f–trajectory, while the second and third vacuum trajectories – to $\alpha_{f'}$ and α_G correspondingly. In the region of large $t > 0$ the effects of mixing are small.

It is interesting that with an account of the quark-gluon mixing the intercept of the Pomeron trajectory is close to the value $j = 1$ corresponding to an exchange by 2 noninteracting gluons.

Up to now I have considered mostly nonperturbative, large distance dynamics of the Pomeron. A small distance dynamics of the Pomeron has been studied in many papers using the QCD perturbation theory (see for example reviews [20]). in the leading log approximation the Pomeron corresponds to a sum of the ladder-type diagrams with exchange of reggeized gluons in the t-channel (BFKL [15] Pomeron). In this approximation the intercept of the Pomeron is equal to

$$\Delta = \alpha_P(0) - 1 = \alpha_s \frac{12}{\pi} ln2 \tag{23}$$

It has been found recently [21] that α_s corrections substantially decrease Δ compared to LLA result. The intercept of the Pomeron depends on the renormalization scheme and scale for α_s. In the "physical" (BLM) scheme values of Δ are in the region $0.15 \div 0.17$.[22] Unfortunately it is very difficult to calculate higher order corrections in PQCD.

Sometimes the BFKL Pomeron is called "hard" Pomeron contrary to the "soft" one. However the equation for the Pomeron singularity contains both nonperturbative effects discussed above and perturbative dynamics. Thus the resulting "physical" pole is a state due to both "soft" and "hard" interactions.

5 Regge cuts. High-energy hadronic interactions

5.1 Multi-Pomeron exchanges

Regge poles are not the only singularities in the complex angular momentum plane. Exchange by several reggeons in the t-channel shown for the Pomeron case in Fig.12 leads to moving branch points (or Regge cuts) in the j-plane. The positions of the branch points for t=0 can be expressed in terms of intercept of the Pomeranchuk pole

$$\alpha_{np}(0) - 1 = n(\alpha_p(0) - 1) = n\Delta \tag{24}$$

Contributions of these singularities to scattering amplitudes $T_n(s, 0) \sim s^{1+n\Delta}$ are especially important at high energies for $\Delta > 0$. The whole series of n-Pomeron exchanges should be summed. An account of these multi-Pomeron exchanges in the t-channel leads to unitarization of scattering amplitudes.

In the framework of 1/N-expansion the n-Pomeron exchange amplitudes are due to topologies with (n-1) handles and are of the order $(1/N^2)^n$.

The Gribov reggeon diagrams technique [23] allows one to calculate contributions of Regge cuts to scattering amplitudes. I shall illustrate this using as

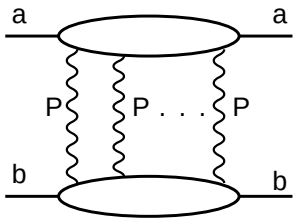

Figure 12: Diagrams with an exchange by several Pomerons in the t=channel.

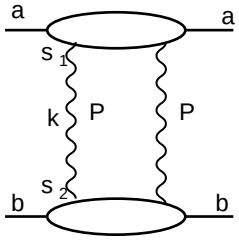

Figure 13: The diagram of two-Pomeron exchange for elastic scattering amplitude.

an example the two-Pomeron exchange contribution to the elastic scattering amplitude. The Pomeron-particle scattering amplitudes, which enter into the diagram of Fig.13, have usual analyticity properties in variables s_i (poles and cuts) and changing the integration in the diagram from d^4k to $ds_1 ds_2 d^2k_\perp/2s$ one can write the diagram of two-Pomeron exchange in the form

$$T_{2P}(s,t) = \frac{i}{2!}\int \frac{d^2k_\perp}{\pi}\eta_p(k_\perp^2)\eta_p((\vec{k}_\perp - \vec{q})^2)$$

$$(\frac{s}{s_0})^{\alpha_P(k_\perp^2)+\alpha_P((\vec{k}_\perp-\vec{q})^2)-2} \times N_a(\vec{k}_\perp,\vec{q})N_b(\vec{k}_\perp,\vec{q}) \qquad (25)$$

The amplitudes $T_{aP,bP}$ decrease faster than $1/s_i$ at large s_i and the contours of integrations on s_i can be transformed in such a way that only discontinuities of these amplitudes at the right hand cut enter into N_a, N_b. The Pomeron-particle scattering amplitudes satisfy to the unitarity condition, and the discontinuities can be expressed as a sum over contributions of intermediate states on mass shell. Thus the two-Pomeron exchange diagram of Fig.13 can be expressed as the sum of diagrams, shown in Fig.14. The diagram of Fig. 14a) corresponds to the P pole contribution to the elastic scattering amplitude, while the diagrams

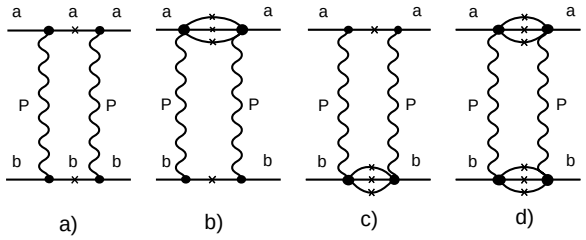

Figure 14: Rescattering diagrams. (Crosses on lines indicate that they are on mass shell).

of Fig. 14 b)-d) are P pole contributions to inelastic diffraction. The diagrams with n-Pomeron exchange in the t-channel can be treated in the same way. The sum of the elastic rescatterings leads to the eikonal formula for the amplitude of ab-scattering in the impact parameter space

$$f_{ab}(s,b) = \frac{i}{2}(1 - exp[2i\delta_P(s,b)]) \tag{26}$$

where $\delta_P(s,b) = \int \frac{d^2q}{2\pi} exp(i\vec{q}\cdot\vec{b}) T_P(s,q_\perp^2)$. In general $f(s,b)$ can be written in the form

$$f(s,b) = \frac{1}{2i}\sum_{n=1}^{\infty} \frac{(-v_p)^n}{n!}\gamma_n \tag{27}$$

where $v_P(s,b) = -2i\delta_P(s,b)$. In the eikonal approximation all $\gamma_n = 1$. All diagrams in Fig.14 have the same sign. This leads to the constraint $\gamma_2 \equiv C > 1$, which means that $|T_{2P}|$ for the contribution of the PP-cut to the amplitude is always larger than the eikonal value . A simplest generalization of the eikonal model, which takes into account also inelastic diffractive intermediate states is so called "quasieikonal" model, where $\gamma_n = C^{n-1}$ and the amplitude $f(s,b)$ has the form

$$f(s,b) = \frac{i}{2C}(1 - exp(-Cv_P)) \tag{28}$$

The function $v_P(s,b) \sim s^{\Delta}$ and it becomes large at very high energies. In this limit the scattering amplitude for elastic scattering $f(s,b) \to i/2$ in the eikonal model (scattering on a black disk) and $f(s,b) \to 1/2C$ in the quasieikonal model (scattering on a grey disc). This property of the quasieikonal model is closely related to the fact that one of the eigen states for the diffractive matrix $\hat{v}_P$ has in this model a zero eigenvalue. This is a crude approximation, which takes into account a big difference in the interaction cross section of hadrons with different transverse sizes. Configurations of quarks inside hadrons

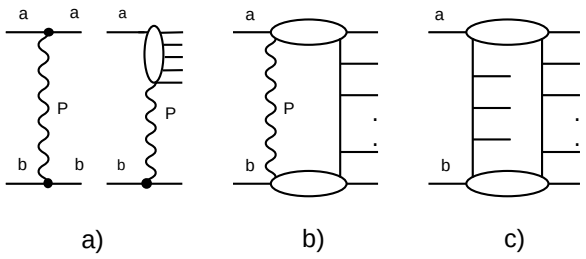

Figure 15: Different contributions to the s-channel cutting of the two-Pomeron exchange diagram.

with small transverse size r have total interaction cross sections $\sim r^2$, because hadrons in QCD interact as color dipoles. There is a distribution of quarks and gluons inside colliding hadrons with different values of r so one can expect that there will be a slow approach to the black disk limit for elastic scattering amplitude as $s \to \infty$. In this limit the effective radius of interaction increases as ln s. Thus total interaction cross sections for the supercritical Pomeron theory have Froissart type behavior $\sigma^{(tot)} \sim ln^2(s)$ as $s \to \infty$.

5.2 AGK-cutting rules

Now we shall discuss the s-channel unitarity for contributions of Pomeron cuts. The connection between different s-channel intermediate states and contribution of cuts to the imaginary part of elastic scattering amplitude is given by Abramovsky, Gribov, Kancheli (AGK)-cutting rules. [24] I shall illustrate them using as an example two-Pomeron exchange amplitude (Fig.13). Its contribution to the imaginary part of the forward elastic ab-scattering amplitude is negative and can be denoted as $T_{2P}(s,b) = -A(s)$ and to the $\sigma^{(tot)}$ as $-\sigma_2$.

There are three different classes of diagrams, which can be obtained by the s-channel cuttings of the diagram of Fig.15. They contribute to different classes of physical processes.

a) The cutting between the Pomerons leads to diffractive processes (both elastic and inelastic), shown in Fig.15 a). Their contributions to the $ImT_{ab}(s,0)$ and $\sigma^{(tot)}$ according to AGK-rules are A(s) and σ_2 correspondingly.

b) Cutting through one of Pomerons (Fig.15 b)) leads to absorptive corrections for the multiperipheral type inelastic production of particles, corresponding to the s-channel content of the Pomeron. AGK rules give for this contribution-4A(s) and $-4\sigma_2$ correspondingly.

c) Cutting through both of Pomerons (Fig.15 c)) leads to a new process,-

production of two multiperipheral chains. According to AGK-rules this contributes 2A(s) to the imaginary part of the forward scattering amplitude and $2\sigma_2$ to the total cross section.

The summary contribution of all these process to the total cross section is $(1-4+2)\sigma_2 = -\sigma_2$.

The AGK rules are formulated [24] for arbitrary diagrams with exchange of n reggeons in the t-channel. They allow to classify all multiparticle configurations and calculate their weights in terms of contributions to forward elastic scattering amplitude (or the corresponding amplitudes in the impact parameter space). For example in the eikonal or quasieikonal models all cross sections (diffractive and inelastic with different number of multiperipheral chains) can be expressed in terms of a single Pomeron exchange contribution to an elastic scattering amplitude.

Let us consider some consequences of these rules for particle production at very high energies.

1) For a sum of all n-Pomeron exchange diagrams of the eikonal-type (without interaction between Pomerons) there is a cancellation of their contributions to the single particle inclusive spectra in the central rapidity region for $n \geq 2$.[24] So only the pole diagram of Fig.6 contributes and inclusive spectra increase with energy as $f^a \sim (s/s_0)^{\Delta}$. This means in particular that a study of an energy dependence of inclusive spectra in the central rapidity region gives more reliable information on the value of Δ, than $\sigma^{(tot)}$, where Pomeron cuts strongly modify energy dependence compared to the pole diagram. Inclusive charged particles density at $y = 0$ for $pp(\bar{p}p)$-collisions has a fast increase with energy and can be described in eikonal-type models with the intercept of the Pomeron in the range $\Delta = 0.12 - 0.14$. The calculation of the total and elastic scattering cross sections in the same model with these values of Δ also leads to a good description of experiment.[25,26] It should be noted that the value of Δ becomes larger ($\Delta \approx 0.2$) if the interaction between Pomerons is taken into account [27] (see below).

2) Pomeron cuts lead to long range correlations in rapidity. Existence of such correlations (for example long range correlations between number of particles produced in the forward and backward hemispheres in the c.m. system) is now firmly established in particle production at high energies.

3) Existence of poliperipheral contributions with several multiperipheral chains leads to broad multiplicity distributions of produced hadrons with the dispersion $D \sim \langle n \rangle$. The s-channel cutting of a single Pomeron leads to a Poisson-type distribution with $\langle n \rangle = \langle n \rangle_P$, for cutting of two Pomerons (Fig.14 c)) the distribution is of the same type but with $\langle n \rangle \approx 2\langle n \rangle_p$ and so on. The summary contribution for cuttings of all n-Pomeron exchange diagrams is broad and

has a complicated form. At not too high energies contributions from different n strongly overlap and multiplicity distributions satisfy to a good accuracy KNO-scaling ($\langle n\rangle\sigma_n/\sigma^{(in)} = f(n/\langle n\rangle)$). However as energy increases KNO scaling is violated. The models based on the reggeon diagrams technique and AGK-cutting rules[25,26] give a good quantitative description of multiplicity distributions .

The theoretical models mentioned above (the Dual Parton Model [26] and the Quark Gluon Strings Model [25] use besides the reggeon theory also 1/N-expansion for interpretation of different reggeon diagrams in QCD. This leads to a very predictive approach to multiparticle production in hadron -hadron, hadron-nucleus and nucleus-nucleus collisions. With a small number of parameters these models allow one to describe total and elastic cross sections, diffraction dissociation, multiplicity distributions, inclusive cross sections for different types of hadrons e.t.c. in a broad region of energies.[25,26]. In the following we shall apply the same approach to DIS in the small x region.

5.3 Interactions between Pomerons

In the eikonal-type models discussed above the diffraction dissociation to the states with not too large masses has been taken into account. The diffractive production of states with large masses is related, as we know from the discussion of diffractive processes, to the diagrams of the type shown in Fig.8 with interaction between Pomerons. Neglect in the first approximation by these interactions is justified by a smallness of triple-Pomeron and 4-Pomeron interaction vertices, found from analysis of diffractive processes.[8] However at very high energies it is necessary to include all these diagrams in order to have a selfconsistent description of high energy hadronic interactions, including large mass diffractive production of particles. It was demonstrated in paper [27] that inclusion of these diagrams leads in most of the cases to predictions which are very close to the results of eikonal type models, however the value of the "bare" Pomeron intercept increases up to the value $\alpha_P(0) \approx 1.2$.

6 Small-x physics

This section is devoted to a problem of small-x physics in deep inelastic scattering (DIS) . This problem became especially actual due to recent experimental investigation of this region at HERA accelerator.

In DIS it is possible to study different asymptotic limits. For a virtuality of the photon $Q^2 \to \infty$ and $x = Q^2/(W^2 + Q^2) \sim 1$ the usual QCD evolu-

tion equations can be applied and Q^2 dependence of the structure functions can be predicted if an initial condition for structure functions at $Q^2 = Q_0^2$ is formulated. On the other hand if Q^2 is fixed and $x \to 0$ (or $\ln(1/x) \to \infty$) the asymptotic Regge limit is relevant. The most interesting question is what is the behavior of DIS in the region where both $\ln(1/x)$ and $\ln(Q^2)$ are large? This is a transition region between perturbative and nonperturbative dynamics in QCD and its study can give an important information on the properties of confinement and its relation to the QCD perturbation theory. The asymptotic Regge limit in DIS can be related to high-energy limit of hadronic interactions and is described in terms of the Pomeranchuk singularity.

Experiments at HERA have found two extremely important properties of small-x physics : a fast increase of parton densities as x decreases [28,29] and the existence of substantial diffractive production in deep inelastic scattering (DIS).[30,31]

A fast increase of $\sigma_{\gamma^* p}^{(tot)}$ as $W^2 \equiv s$ increases at large Q^2 observed experimentally [28,29] raises a question: whether there are two different Pomerons – "soft" and "hard"? From the discussion of the Pomeron in QCD above it follows that there are no theoretical reasons for such a situation and most probably the rightmost pole in the j–plane is generated by both "soft" and "hard" dynamics. I shall assume that there is one ("physical") Pomeron pole with the same $\alpha_P(0)$ as it was determined from high–energy hadronic interactions with an account of many–Pomeron cuts. On the other hand the effective intercept, which depends on relative contribution of multi–Pomeron diagrams, can be different in different processes.

In paper[32] it was suggested that the increase of the effective intercept of the Pomeron, $\alpha_{eff} = 1+\Delta_{eff}$, as Q^2 increases from zero to several GeV^2 is mostly due to a decrease of shadowing effects with increasing Q^2. A parametrization of the Q^2 dependence of Δ_{eff} such that $\Delta_{eff} \approx 0.1$ for $Q^2 \approx 0$ (as in soft hadronic interactions) and $\Delta_{eff} \approx 0.2$ (bare Pomeron intercept) for Q^2 of the order of a few GeV^2, gives a good description of all existing data on $\gamma^* p$ total cross-sections in the region of $Q^2 \leq 5 \div 10$ GeV^2.[32,33] At larger Q^2 effects due to QCD evolution become important. Using the above parametrization as the initial condition in the QCD evolution equation, it is possible to describe the data in the whole region of Q^2 studied at HERA.[32,34]

In the reggeon approach discussed above there are good reasons to believe that the fast increase of the $\sigma_{\gamma^* p}$ with energy in the HERA energy range will change to a milder increase at much higher energies. This is due to multi–Pomeron effects, which are related to shadowing in highly dense systems of partons - with eventual "saturation" of densities. This problem has a long history (for reviews see [20,35]) and has been extensively discussed in recent

years.[36] It is closely connected to the problem of the dynamics of very high-energy heavy ion collisions.[37]

This problem was investigated recently in our paper [38], where reggeon approach was applied to the processes of diffractive $\gamma^* p$ interaction. It was emphasized in the previous section that in the reggeon calculus [23] the amount of rescatterings is closely related to diffractive production. AGK-cutting rules [24] allow to calculate the cross-section of inelastic diffraction if contributions of multi-Pomeron exchanges to the elastic scattering amplitude are known. Thus, it is very important for self-consistency of theoretical models to describe not only total cross sections, but, simultaneously, inelastic diffraction. In particular in the reggeon calculus the variation of Δ_{eff} with Q^2 is related to the corresponding variation of the ratio of diffractive to total cross sections. In the paper [38] an explicit model for the contribution of rescatterings was constructed which leads to the pattern of energy behavior of $\sigma^{(tot)}_{\gamma^* p}(W^2, Q^2)$ for different Q^2 described above. Moreover, it allows to describe simultaneously diffraction production by real and virtual photons. In this model it is possible to study quantitatively a regime of "saturation" of parton densities.

Let us discuss briefly the qualitative picture of diffractive dissociation of a highly virtual photon at high energies. It is convenient to discuss this process in the lab. frame, where the quark-gluon fluctuations of a photon live a long time $\sim 1/x$ (Ioffe time [39]). A virtual photon fluctuates first to $q\bar{q}$ pair. There are two different types of configurations of such pair, depending on transverse distance between quarks (or $k_\perp$).
a) Small size configurations with $k^2_\perp \sim Q^2$. These small dipoles ($r \sim 1/k_\perp \sim 1/Q$) have a small ($\sim r^2$) total interaction cross section with the proton.
b) Large size configurations with $r \sim 1/\Lambda_{QCD}$ and $k_\perp \sim \Lambda_{QCD} \ll Q$. They have a large total interaction cross section, but contribute with a small phase space at large Q^2, because these configurations are kinematically possible only if the fraction of longitudinal momentum carried by one of the quarks is very small $x_1 \sim k^2_\perp/Q^2 \ll 1$. This configuration corresponds to the "aligned jet", introduced by Bjorken and Kogut.[40]

Both configurations lead to the same behaviour of $\sigma_{\gamma^* p} \sim 1/Q^2$, but they behave differently in the process of the diffraction dissociation of a virtual photon [41,42]. The cross section of such a process is proportional to a square of modulus of the corresponding diffractive amplitude and for a small size configuration it is small ($\sim 1/Q^4$). For large size configurations a smallness is only due to the phase space and the inclusive cross section for diffractive dissociation of a virtual photon decreases as $1/Q^2$, i.e. in the same way as the total cross section. This is true only for the total inclusive diffractive cross section, where characteristic masses of produced states are $M^2 \sim Q^2$. For

exclusive channels with fixed mass (for example production of vector mesons) situation is different and these cross sections decrease faster than $1/Q^2$ at large Q^2.

Inclusive diffractive production of very large masses ($M^2 \gg Q^2$) can be described in the first approximation by triple-Regge diagrams (Fig.8).[43] From the point of view of the quark-gluon fluctuation of the fast photon triple-Pomeron contribution corresponds to diffractive scattering of very slow (presumably gluonic) parton, which has a small virtuality.

The model [38] uses the picture of diffraction dissociation of a virtual photon outlined above and is a natural generalization of models used for the description of high-energy hadronic interactions. The interaction of the small size component in the wave function of a virtual photon is calculated using QCD perturbation theory. The main parameter of the model - intercept of the Pomeron was fixed from a phenomenological study of these interactions discussed above ($\Delta_P = 0.2$) and was found to give a good description of $\gamma^* p$-interactions in a broad range of Q^2 ($0 \leq Q^2 < 10\ GeV^2$). Another important parameter of the theory, the triple Pomeron vertex, obtained from a fit to the data ($r^{(0)}_{PPP}/g^P_{pp}(0) \approx 0.1$) is also in reasonable agreement with the analysis of soft hadronic interactions.[27,43] The description of $\sigma^{(tot)}_{\gamma^* p}$ as a function of s for different values of Q^2 (experimental data are from H1 [28], ZEUS [29]) is shown in Fig.16. Diffraction dissociation of a virtual photon is usually presented as a function of Q^2, M^2 (or $\beta = Q^2/(M^2+Q^2)$) and $x_P = x/\beta = (M^2+Q^2)/(W^2+Q^2)$. Description of HERA data on diffractive dissociation [31] in the model is shown in Fig.17. The model reproduces experimental data quite well. It can be used to predict structure functions and partonic distributions at higher energies or smaller x, which will be accessible for experiments at LHC.

7 Acknowledgments

I am grateful to K.Boreskov, A.Capella, V.Fadin, E.G. Ferreiro, O.V. Kancheli, J.H. Koch, G. Korchemski, E. Levin, L.N. Lipatov, C. Merino, C.A. Salgado, K.A. Ter-Martirosyan and J. Tran Thanh Van for useful discussions.
This work is supported in part by the grants RFFI-98-02-17463 and NATO OUTR.LG 971390.

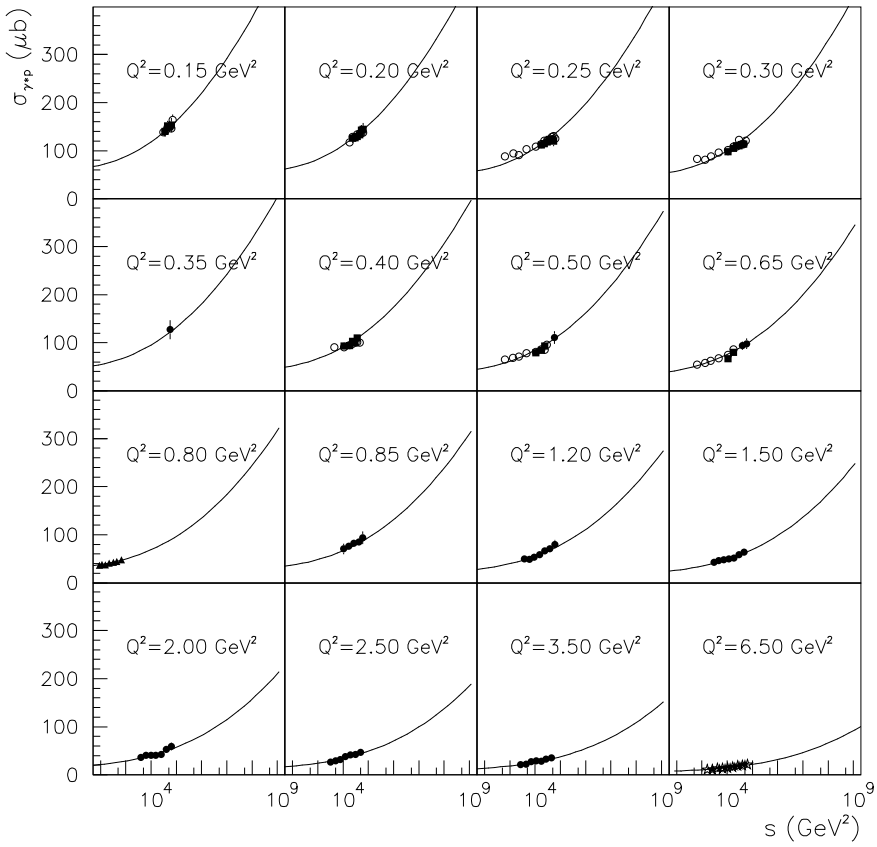

Figure 16: $\sigma^{(tot)}_{\gamma^* p}$ as a function of s for different values of Q^2 compared with experimental data.

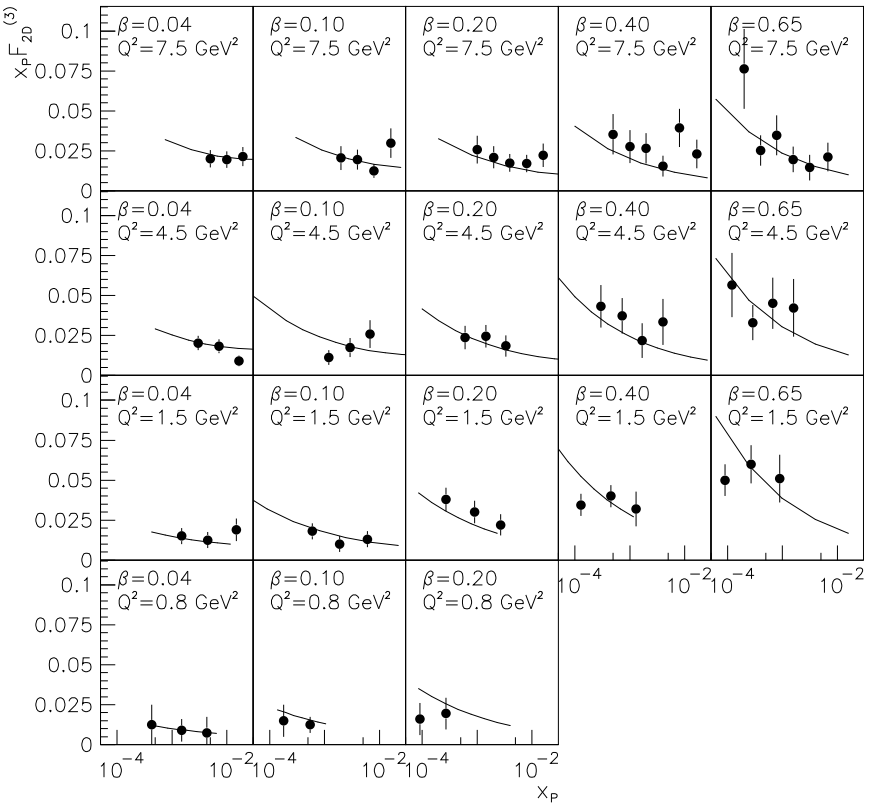

Figure 17: The diffractive structure function $x_P F_2^{D(3)}$ as a function of x_P for fixed values of Q^2 and $\beta = Q^2/(Q^2 + M^2)$.

References

1. V.N. Gribov, *ZhETF***41**, 667 (1961). .
2. G.F. Chew and S.C. Frautschi, *Phys. Rev. Lett.* **7**, 394 (1961).
   R. Blankenbecler and M. Goldberger, *Phys. Rev.* **126**, 766 (1962).
3. T. Regge, *Nuovo Cimento* **14**, 951 (1959).
4. M. Froissart, *Phys. Rev.* **123**, 1053 (1959).
5. D. Amati, A. Stanghellini and S. Fubini, *Nuovo Cimento* **26**, 896 (1962).
6. A.H. Mueller, *Phys. Rev.* D **23**, 2963 (1970).
   O.V. Kancheli, *JETP Lett.* **11**, 267 (1970).
7. A.B. Kaidalov, K.A. Ter-Martirosyan, *Nucl. Phys.* B **75**, 471 (1974).
8. A.B. Kaidalov, *Phys. Rep.* **50**, 157 (1979).
   G. Alberi and G. Goggi, *Phys. Rep.* **74**, 1 (1981).
   K. Goulianos, *Phys. Rep.* **101**, 169 (1983).
9. G. t'Hooft, *Nucl. Phys.* B **72**, 461 (1974).
10. G. Veneziano, *Phys. Lett.* B **52**, 220 (1974); *Nucl. Phys.* B **117**, 519 (1976).
11. A.B. Kaidalov, *Surveys in High Energy Phys.* **13**, 265 (1999).
12. A. Dubin, A. Kaidalov, Yu. Simonov, *Phys. Lett.* B **323**, 41 (1994) ; *Yad. Fiz.* **56**, 213 (1993) .
13. Yu.A. Simonov, *Nucl. Phys.* B **307**, 512 (1988) ; *Yad. Fiz.* **54**, 192 (1991) .
14. F.E. Low, *Phys. Rev.* D **12**, 163 (1975).
    S. Nussinov, *Phys. Rev. Lett.* **34**, 1286 (1975).
15. L. N. Lipatov,*Sov. J. Nucl. Phys.* **23**, 338 (1976).
    E. A. Kuraev, L. N. Lipatov, V.S. Fadin, *Sov. Phys. JETP* **45**, 199 (1977).
    Y. Y. Balitsky, L. N. Lipatov, *Sov. J. Nucl. Phys.* **28**, 822 (1978).
    L.N. Lipatov, *Nucl. Phys.* B **365**, 614 (1991).
16. C. Morningstar, M. Peardon, *Phys. Rev.* D **60**, 034509 (1999) .
17. M. Teper, hep-th/9812187
18. Yu.A. Simonov, *Phys. Lett.* B **249**, 514 (1990).
19. A.B. Kaidalov, Yu.A. Simonov, *Phys. Lett.* B **477**, 163 (2000); hep-ph/9911291.
20. L. V. Gribov, E. M. Levin and M. G. Ryskin, *Phys. Rep.* **100**, 1 (1983).
    E. Laenen and E. Levin, *Ann. Rev. Nucl. Part.* **44**, 199 (1994).
    A. H. Mueller, hep-ph/9911289.
21. V. S. Fadin, L. N. Lipatov, *Phys. Lett.* B **429**, 127 (1998).
    G. Camici, M. Ciafaloni, *Phys. Lett.* B **430**, 349 (1998).
22. S.J.Brodsky *et al*, *JETP Lett.* **70**, 155 (1999).

23. V. N. Gribov, *ZhETF* **57**, 654 (1967).
24. V. A. Abramovsky, V. N. Gribov and O. V. Kancheli, *Sov. J. Nucl. Phys.* **18**, 308 (1974).
25. A. Kaidalov, in *"QCD at 200 TeV"*, ed. L.Cifarelli and Yu. Dokshitzer, Plenum Press (1992), p.1.
26. A. Capella, U. Sukhatme, C.-I. Tan and J. Tran Thanh Van, *Phys. Rep.***236**, 225 (1994).
27. A. B. Kaidalov, L. A. Ponomarev and K. A. Ter-Martirosyan, *Sov. J. Nucl. Phys.* **44**, 468 (1986).
28. T.Ahmed *et al* (H1 Collaboration), *Phys. Lett.* B **299**, 374 (1992);
    C. Adloff *et al* (H1 Collaboration), *Nucl. Phys.* B **497**, 3 (1997).
29. M.Derrick *et al* (ZEUS Collaboration), *Phys. Lett.* B **293**, 465 (1992);
    J. Breitweg *et al* (ZEUS Collaboration), *Phys. Lett.* B **407**, 432 (1997);
    J. Breitweg *et al* (ZEUS Collaboration), Preprint DESY 00-071.
30. M. Derrick *et al* (ZEUS Collaboration), *Z. Phys.* C **72**, 399 (1996).
31. C. Adloff *et al* (H1 Collaboration), *Z. Phys.* C **76**, 613 (1997).
32. A. Capella, A. Kaidalov, C. Merino, J. Tran Thanh Van, *Phys. Lett.* B **337**, 358 (1994).
33. A. Kaidalov, C. Merino, *Eur. Phys. J.* **C10**, 153 (1999).
34. A. Kaidalov, C. Merino, D. Perterman, hep-ph/9911331.
35. A. B. Kaidalov, *Surveys High Energy Phys.* **9**, 143 (1996).
36. A. H. Mueller, *Nucl. Phys.* B **437**, 107 (1995).
    A. L. Ayala, M. B. Gay Ducati and E. M. Levin, *Phys. Lett.* B **388**, 188 (1996) ; *Nucl. Phys.* B **493**, 305 (1997).
    E. Gotsman, E. Levin and U. Maor, *Nucl. Phys.* B **493**, 354 (1997) ; *Phys. Lett.* B **425**, 369 (()1998) ; **B452**, 387 (1999).
    E. Gotsman, E. Levin, U. Maor and E. Naftali, *Nucl. Phys.* B **539**, 535 (1999).
    L L. Frankfurt, W. Kopf and M. Strikman, *Phys. Rev.* D **57**, 512 (1998) ; **D54**, 3194 (1996).
    M. Mac Dermott, L. L. Frankfurt, V. Guzey and M. Strikman, hep-ph 9912547.
    K. Golec-Biernat and M. Wüsthoff, *Phys. Rev.* D **59**, 014017 (1999) ; **D60**, 114023 (1999).
    A. H. Mueller, *Eur. Phys. J.* **A1**, 19 (1998).
37. L. Mc Lerran and R. Venugopalan, *Phys. Rev.* D **49**, 2233, 3352 (1994) ; **50**, 2225 (1994) ; **53**, 458 (1996).
    J. Jalilian-Marian et al., *Phys. Rev.* D **59**, 014014, 034007 (1999).
    A. Kovner, L. Mc Lerran and H. Weigert, *Phys. Rev.* D **52**, 3809, 6231 (1995).

Yu. V. Kovchegov and A. H. Mueller, *Nucl. Phys.* B **529**, 451 (1998).
Yu. V. Kovchegov, A. H. Mueller and S. Wallon, *Nucl. Phys.* B **507**, 367 (1997).
A. H. Mueller, *Nucl. Phys.* B **558**, 285 (1999).
A. Capella, A. Kaidalov, J. Tran Thanh Van, *Heavy Ion Phys.* **9**, 169 (1999).
38. A. Capella, E. Ferreiro, A.B. Kaidalov and C.A. Salgado, hep-ph/0005049, hep-ph/0006233.
39. B.L. Ioffe, *Phys. Lett.* B **30**, 123 (1969).
40. J. D. Bjorken and J. B. Kogut, *Phys. Rev.* D **8**, 1341 (1973).
41. L. L. Frankfurt and M. Strikman, *Phys. Rep.* **160**, 235 (1988).
42. N. N. Nikolaev and B. G. Zakharov, *Z. Phys.* C **49**, 607 (1990).
43. A. Capella, A. Kaidalov, C. Merino, J. Tran Than Van, *Phys. Lett.* B **343**, 403 (1995).
A. Capella, A. Kaidalov, C. Merino, D. Perterman, J. Tran Than Van, *Phys. Rev.* D **53**, 2309 (1996).